Loughborough University

This item was submitted to Loughborough's Research Repository by the author.
Items in Figshare are protected by copyright, with all rights reserved, unless otherwise indicated.

Asperity level frictional interactions of cylinder bore materials and lubricant composition

PLEASE CITE THE PUBLISHED VERSION

https://doi.org/10.1177/1350650120903928

PUBLISHER

SAGE Publications

VERSION

VoR (Version of Record)

PUBLISHER STATEMENT

This is an Open Access Article. It is published by Sage under the Creative Commons Attribution-NonCommercial 4.0 International Licence (CC BY-NC). Full details of this licence are available at: https://creativecommons.org/licenses/by-nc/4.0/

LICENCE

CC BY-NC 4.0

REPOSITORY RECORD

Forder, Michael, Jamal Umer, Nick Morris, Ramin Rahmani, Sebastian Howell-Smith, and Homer Rahnejat. 2020. “Asperity Level Frictional Interactions of Cylinder Bore Materials and Lubricant Composition”. Loughborough University. https://hdl.handle.net/2134/11591292.v1.

Check for updates

Original Article

Institution of MECHANICAL ENGINEERS
Journal of ENGINEERING TRIBOLOGY

Proc IMechE Part J:
J Engineering Tribology
2021, Vol. 235(4) 679–686
© IMechE 2020

Article reuse guidelines:
sagepub.com/journals-permissions
DOI: 10.1177/1350650120903928
journals.sagepub.com/home/pij

Asperity level frictional interactions of cylinder bore materials and lubricant composition

Michael Forder, Jamal Umer, Nicholas Morris, Ramin Rahmani, Sebastian Howell-Smith and Homer Rahnejat

Abstract

Parasitic frictional losses in internal combustion engines of race vehicles adversely affect their performance. A significant proportion of these losses occur within the piston-cylinder system. This paper presents a study of the compatibility of cylinder bore surface materials with typical lubricant base constituent stock (poly alpha olefin and polyolester) as well as a fully formulated lubricant. Nanoscale boundary friction is measured using lateral force microscopy. The effect of material properties, nanoscale roughness and lubricant species upon underlying mechanisms of generated friction is presented. Advanced cylinder materials and coatings and lubricant molecular species used for high performance engines are investigated, and an integrated approach not hitherto reported in literature.

Keywords

Atomic force microscope, lateral force microscopy, lubricant-surface combination, friction

Date received: 29 July 2019; accepted: 20 December 2019

Introduction

For motorsport applications, where engine operating conditions are often reasonably predictable, and, in some cases, entirely controllable, focus can be placed upon the enhanced performance through reduced friction of in-cylinder components. Reduction of gradual wear is a secondary concern as competition engines are often rebuilt based on a mileage or a measured unit time interval, which in some instances can be less than 200 miles or 10 h running under race conditions. During such operations, frequent inspection of any indicators of wear can be made and some remedial actions undertaken.

To highlight the importance of reducing friction in the piston-cylinder subsystem, it is necessary to consider the magnitude of the accrued losses. A typical spark ignition engine has an inefficiency, which may be as high as 60–70%. Of the underlying losses, a large proportion is thermal, but as much as 33% can be attributed to engine friction. Almost half of these losses can be attributed to the frictional losses related to the piston assembly, 7–8% of which occurs at the interface between piston compression rings and the cylinder liner.

With the development of lightweight and durable aluminium alloys, the cast-iron cylinder blocks (with no requirement for liners or inserts) have been largely replaced. However, these new lightweight castings require either spray coatings or pressed-in inserts to prevent excessive cylinder bore wear and friction. As a result, designers have turned their attention to an array of selected spray coatings, electro-plates or liners which replicate or outperform cast-iron tribologically.

Engine and component level testing[1–4] has been shown to be an excellent methodology to benchmark alternative lubricant-surface combinations. In recent years, the development of nanoscale experimental techniques, such as surface force apparatus techniques and atomic force microscopy (AFM), has led to an improved fundamental understanding of asperity level interactions and confined fluid behaviour. The fluid-cell AFM has become an important tool for the investigation of the growth and frictional properties of surfaces, self-assembled monolayers

Wolfson School of Mechanical, Electrical and Manufacturing Engineering, Loughborough University, Leicestershire, UK

Corresponding author:
Nicholas Morris, Wolfson School of Mechanical, Electrical and Manufacturing Engineering, Loughborough University, Leicestershire, UK.
Email: N.J.Morris@Lboro.ac.uk

and tribofilms.[5–12] Pidduck and Smith[5] and Leighton et al.[9] showed that AFM can be used to investigate generated tribofilms, generated through the use of tribometry. A range of lubricant formulations containing ZDDP were investigated on EN31 hardened steel surface.[5] Miklozic and Spikes[6] conducted tests for various lubricant formulations, including the dispersants; MoDTC and ZDDP with both tribometers and AFM. Tests are conducted on a single steel-type substrate (i.e. AISI 52100), demonstrating the variation in surface film formation and frictional properties of the two additives under investigation. The same approach was reported by Leighton et al.[9] for a base oil and formulated lubricants with different viscosity modifiers. Also, Bhushan et al.[7] investigated the friction and wear resistance of ionic lubricants for MEMS devices. Again, they showed that varying the lubricants' composition altered the performance with a single material type (in that case, silicon). Campen et al.[8] investigated the formation of various fatty acids using lateral force microscopy (LFM) on mica surfaces. The study demonstrated fluid-cell AFM to be a suitable method for investigating and elucidating the tribological behaviour of surfaces and boundary films. These investigations have significantly advanced the understanding of thin confined fluid-film lubrication behaviour. Styles et al.[11] used LFM to determine the boundary shear characteristics of various cylinder liner surface types under dry conditions, whilst Bewsher et al.[12] used pieces of real cylinder liners subjected to long-term dynamometric testing together with sample lubricants in fluid-cell LFM. Most investigations have predominantly focused on varying the lubricant additives, whilst using the same surface specimen.

This paper investigates asperity-level interactions and lubricant-surface synergies using fluid-cell LFM. Five sample surfaces with different coatings, commonly used for automotive cylinder liners, particularly for high performance engines, are investigated in the presence of poly alpha olefin (PAO), polyolester (POE) and a mixture of both with a fully formulated lubricant.

Materials and method of measurement

LFM was conducted using a Brucker Dimension 3100 Atomic Force Microscope (AFM), controlled by Digital Instruments Nano Scope 614r1 software. The hardware is mounted on an anti-vibration platform in a laboratory with a controlled atmosphere of 20 °C (±0.5 °C) and relative humidity of 50% (±5%) with a barometric pressure of 101.345 kPa. Non-conductive silicon nitride DNP-10 tips (cantilever D) with a tip radius of 20 ± 1 nm and a cantilever arm stiffness of 0.06 N/m are used for all the LFM tests. Each test constitutes 256-line scans over an area of 1 μm^2 with the tip sliding speed of 1 μm/s. The normal tip load was increased between successive tests, with the same lubricant-surface combination, from 10 to 50 nN in increments of 2.5 nN. The mean contact pressures are found using the classical Hertzian contact theory for concentrated point contacts, for the upper and lower bounds of the applied load corresponding pressures shown in Table 1. For the results shown in Table 1 the surface roughness is ignored and only the AFM tip curvature is considered to contribute to the equivalent radius. The values for the elastic moduli for each contacting surface are reported by Umer et al.[13]

Before each measurement, a blind calibration procedure is used[10,11] with a TGF 11 monocrystalline silicon grating. Friction was measured using the trace-minus-retrace method, where

$$C_F = \frac{TMR[V]}{L[nN] \times 0.19} \tag{1}$$

Friction is then obtained as

$$F_f[nN] = \frac{TMR[V]}{C_F} \tag{2}$$

Asperity level frictional performance of a combination of five surface types with four formulated lubricants, which are used for automotive cylinder bore surfaces, is studied here. For this purpose, an AFM in LFM is used.

Tables 2 and 3 provide the specifications of sample surfaces, substrate materials and any applied coatings. The listed coatings comprise a wide range of commonly used surfaces for advanced cylinder bores or liner inserts. These include nickel silicon carbide (Ni-SiC_2), diamond-like carbon (DLC), ferro molybdenum (FeMo), titanium dioxide (TIO_2) and aluminium oxide (PEO). These coatings are applied to bespoke flat specimen of dimensions 100 × 50 × 8 mm (Table 3).

Any variations in surface topography of various samples are minimised as far as possible. The DLC-coated sample is used as the topographic baseline (datum), whilst the other surfaces were lapped using a 9 μm polycrystalline diamond polishing paste to attain a comparable surface finish to the DLC sample. The microscale roughness parameters are listed in Tables 2 and 5. The measurements were made using an Alicona focus variation microscope using a 100 × magnification objective.

Four different lubricants are used for the current investigation (Table 4). The first two are synthetic non-polar PAO and a POE, both of which are typical base stock components used in commercial

Table 1. Predicted Tip contact pressures.

Pressure	$NiSiC_2$	DLC	FeMo	TiO_2	PEO
(10 nN) GPa	2.6	3.6	3.2	3.4	2.3
(50 nN) GPa	4.4	6.2	5.4	5.8	3.9

Table 2. Surface coatings.

Sample	Ni-SiC_2	DLC	FeMo	TiO_2	PEO
Coating	Electroplated nickel with co-deposited silicon particulate	Thin film vacuum deposited diamond like carbon	High energy thermally sprayed iron and molybdenum	High energy thermally sprayed TIO_2	High energy 'plasma' anodized
Surface finish as deposited Sq (nm)	N/A	44	N/A	N/A	N/A
Surface finish as lapped Sq (nm)	38	N/A	108	84	29
Thickness as finished (μm)	70	2	400	400	10

Table 3. Substrate materials.

Sample	Ni-SiC_2	DLC	FeMo	TiO_2	PEO
Classification	BS970: 1991 817M40T	BS970: 1991 817M40T	BS970: 1991 817M40T	BS970: 1991 817M40T	AA 4032 T6
Processed	Alloy steel quenched and tempered	Alloy steel quenched and tempered	Alloy steel quenched and tempered	Alloy steel quenched and tempered	Aluminium alloy solution treated and artificially aged

Table 4. Lubricants.

Serial number	Description	Kinematic viscosity (40 and 100°C) cSt	Additional information
PAO	Low viscosity synthetic base PAO	31.0 and 5.8	Viscosity index 138
PEO	Synthetic base POE	19.0 and 4.3	Viscosity index 136
FF	Fully formulated commercial 0W40 oil	70.8 and 12.9	Viscosity index 186
PAO/POE	Blend of PAO and ester lubricants	30.7 and 5.8	Blended to 50:1 by wt. ratio

automotive engine oils. In addition, a fully formulated lubricant, containing PAO, POE, a viscosity modifier and an additive package is used. The fully formulated oil contains a molybdenum-based inorganic friction modifier and an anti-wear additive containing zinc. The mixture is created with a ratio of 50:1 PAO to POE. These base stocks were mixed at 65 °C for 6 h.

The AFM tip radius was measured using a TGT1 silicon wafer with a calibrated surface geometry. The tip was scanned over 20 peaks, with the deconvolution of the measured data, yielding the tip radius.

Initially, the frictional performance of each surface was investigated without the presence of a lubricant (nominally dry LFM). Each sample surface was subsequently divided into four equal sections along its length, with each partitioned area tested in the presence of PAO, PEO, PAO/POE and the fully formulated lubricant, respectively (fluid-cell LFM). This partitioning is carried out in order to prevent any cross-contamination at the various lubricant-sample interfaces. The sample surfaces were thoroughly cleaned prior to each test with petroleum ether (40–60). The calibration procedure is carried out for all wet conditions for topography and friction in all the four sections of all the specimens. Each test (lubricant-surface combination) is repeated three times at different locations within the apportioned regions. A fluid cell is used to keep any lubricant meniscus action away from the vicinity of the tip-sample contact, thus mitigating any potential capillary adhesion, affecting the measurements.

Contact mechanics

The conjunction of the AFM tip-to-a sample surface is subjected to mixed regime of lubrication under suitable conditions.[14] Therefore, the generated friction is expected to be due to the combined result of direct interfacial interaction of contacting surfaces (boundary friction) and friction of a thin fluid film (viscous friction). In ultra-thin film conjunction of LFM, the boundary friction is caused by the shear strength of the interface between the surfaces (τ_a) and viscous shear stress (τ_v) of any formed fluid film.[14] Contact friction can be determined through specifying the proportion of the two shear stresses. This can be

determined by the ratio of the real contact area (α) characterised by the direct contact of the contiguous real rough surfaces and the apparent area of contact, A. Thus[14–16]

$$F = A[\tau_a \alpha + \tau_v(1-\alpha)] \tag{3}$$

where

$$\alpha = \frac{A_a}{A} \tag{4}$$

The Bowden and Tabor's model,[15] described above, has been used by Tambe and Bhushan[14] and Gohar and Rahnejat[16] to effectively predict the generated friction in nanoscale contacts, including at the conjunction of an AFM tip and a sample. It has been shown that the apparent contact area, A, created between an AFM tip and a sample can be reasonably represented by the classical continuum contact mechanics theory.[17–19] Contact adhesion is largely mitigated in the presence of a lubricant in fluid-cell LFM. Therefore, it is reasonable to determine the apparent area of contact using the classical Hertzian contact mechanics[16,20,21]

$$A = \pi\left(\frac{3LR}{4E^*}\right)^{3/2} \tag{5}$$

where the reduced equivalent radius of the contacting pair: the AFM tip against a semi-infinite elastic half-space (a sample surface) is

$$\frac{1}{R} = \frac{1}{R_1} + \frac{1}{R_2} \tag{6}$$

And the equivalent (composite) modulus of elasticity of the elastic half-space becomes

$$\frac{1}{E^*} = \frac{1-\upsilon_1^2}{E_1} + \frac{1-\upsilon_2^2}{E_2} \tag{7}$$

The composite elastic modulus, E^*, for the materials used in this study is taken from AFM measurements reported by Umer et al.[19] To determine the real contact area, A_a, the model proposed by Greenwood and Williamson[22] is used. In this model, real contact area and the asperity load-carrying capacity are given as

$$A_a = \pi\eta\sigma_s\beta A e^{-h} \tag{8}$$

$$L = A\left(\frac{\sigma_s}{\beta}\right)^{\frac{1}{2}} E^* \pi^{\frac{1}{2}} \eta\sigma_s\beta e^{-h} \tag{9}$$

where the roughness parameter $\eta\sigma_s\beta$ comprises the asperity peak areal density, the standard deviation of summit heights and the average asperity peak radius.

Combining equations (5), (8) and (9), the fraction of the real contact area can be determined as

$$\alpha = \frac{A_a}{A} = \frac{8\sqrt{3}}{9\sqrt{\pi}}\sqrt{\frac{\beta}{\sigma_s}}\frac{\sqrt{E^*}}{R^{\frac{3}{2}}\sqrt{L}} \tag{10}$$

Isolating the surface roughness and material property parameters in equation (10), it can be observed that the real contact area fraction between the AFM tip and the surface is a function of surface elastic modulus, the standard deviation of summit heights and average radius of curvature as

$$\alpha \propto \sqrt{\frac{\beta}{\sigma_s}}\frac{\sqrt{E^*}}{R^{\frac{3}{2}}} \tag{11}$$

Homola et al.[23] showed that the interfacial shear strength of the contact in the absence of a lubricant can be approximated by the cobblestone model as

$$\tau_a = \varepsilon\left(\frac{2\gamma}{Z_o}\right) \tag{12}$$

where Z_o is the equilibrium atomic spacing, indicating the lateral distance moved through dislocation in order to initiate any sliding motion. By combining the surface-specific terms in equation (11) with equation (12), the boundary friction component in Bowden and Tabor's relationship (equation (3)) would be proportional to the surface-dependent parameters as well as surface energy as another surface-dependent parameter, thus

$$\tau_a\alpha \propto \sqrt{\frac{\beta}{\sigma_s}}\frac{\sqrt{E^*}}{R^{\frac{3}{2}}}\gamma \tag{13}$$

The surface-specific equilibrium atomic spacing parameter, Z_o, is not included in the proportionality relationship (13) as a reliable method to measure its value and is not available to the authors.

Results and discussion

Friction is obtained using LFM on the five sample surfaces commonly used for automotive cylinder bores, particularly for high performance applications and in the presence of four lubricant types; two of which are constituent components of the lubricant base stock (i.e. PAO and POE), another is a mixture of the two (i.e. PAO and POE), and, finally, a fully formulated lubricant: 0W40 (FF).

Figure 1 shows the measured friction for each lubricant in combination with the various sample surfaces.

Figure 1(a) is for the case of the POA fluid. The results show the influence of surface type upon frictional behaviour when wetted with the PAO. This finding is repeated in the case of all lubricant variants. In all cases, there is a near linear relationship

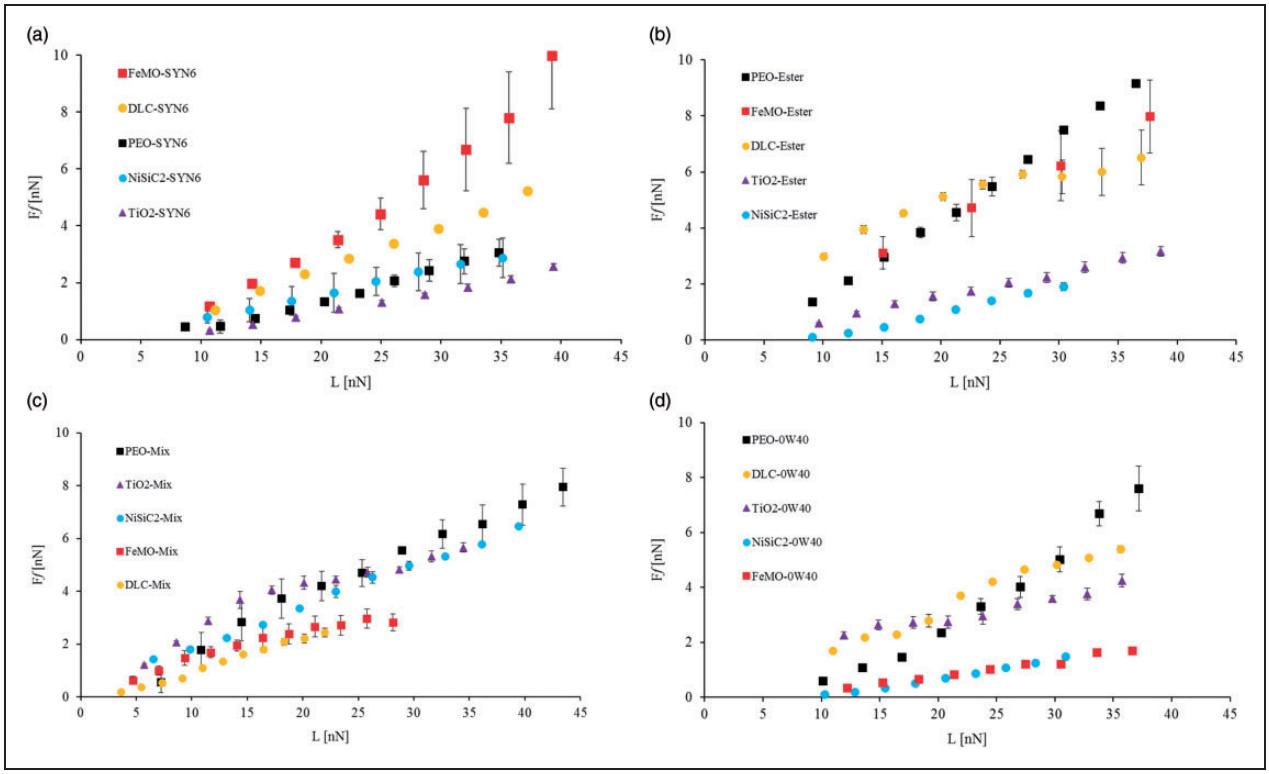

Figure 1. Variation of friction with normal load for different surface coatings in the presence of (a) PAO, (b) POE, (c) PAO and POE mix and (d) fully formulated oil.

between the load and the measured interfacial friction. The slope is analogous to the coefficient of friction by definition. Therefore, a higher slope constitutes greater friction. It is shown that TIO_2 coating, when paired with PAO, produces the lowest coefficient of friction.

Figure 1(b) displays the interfacial friction of sample surfaces wetted by the POE fluid. Again, as with the surfaces wetted with the PAO oil (Figure 1(a)), there is a clear distinction in frictional behaviour of the tested surfaces. The interfacial friction for the FeMo, TiO_2 and DLC surfaces does not appear to be directly proportional to the applied load (as is the case in Figure 1(a)). Such a result suggests slip at the lubricant-surface boundaries as also shown by Fillot et al.[24] The same deviation from linearity is also noted in the presence of a mixture of the PAO and POE fluids for the FeMO, DLC, TiO_2 and PEO samples (Figure 1(c)). The relative frictional performance of the sample surfaces shows that neither constituent fluid mixtures (PAO or POE) dominate the characteristic responses in Figure 1(a) or (b). There appears to be some synergistic or antagonistic interactions, which are commonplace with such lubricant species.

Figure 1(d) shows the interfacial frictional behaviour when each surface is wetted with a fully formulated commercial lubricant. As it would be expected, the two most common piston liner materials/coatings for high performance applications; FeMO and $NiSiC_2$ show the lowest coefficient of friction. Fully formulated lubricants, containing surface-active species, such as friction modifiers, allow $NiSiC_2$ and ferro molybdenum oxide to attain lower coefficients of friction. From similar experiments in literature, employing similar contact types and conditions (Gosvami et al.[25]) at elevated temperatures and higher shear, a large number of sliding cycles are required in order to generate a tribofilm. Due to the relatively low temperature in the current tests and a limited number of sliding cycles, there is a low chance of tribofilm formation of any significant thickness.

A comparison of the measured coefficients of friction thus far with independently (separately) measured surface parameters is shown in Figure 2. The surface parameter selected is provided in equation (13) and is referred to as the boundary friction propensity parameter. The trend in the coefficient of friction variation with this parameter gives an indication of the influence of intervening a lubricant layer upon the mechanics of contact of all the sample surfaces. The surface roughness parameters required for this analysis are measured using AFM (Table 4) and post-processed to remove any long wavelength surface forms. The results for the surface energy, asperity radius of curvature and RMS roughness are listed in Table 5.

The data presented in Table 5 are those measured at a length scale limited by the machines used to measure them. The length scales over which the measurements are taken are close to, but not completely appropriate, for the theory described in the analytical

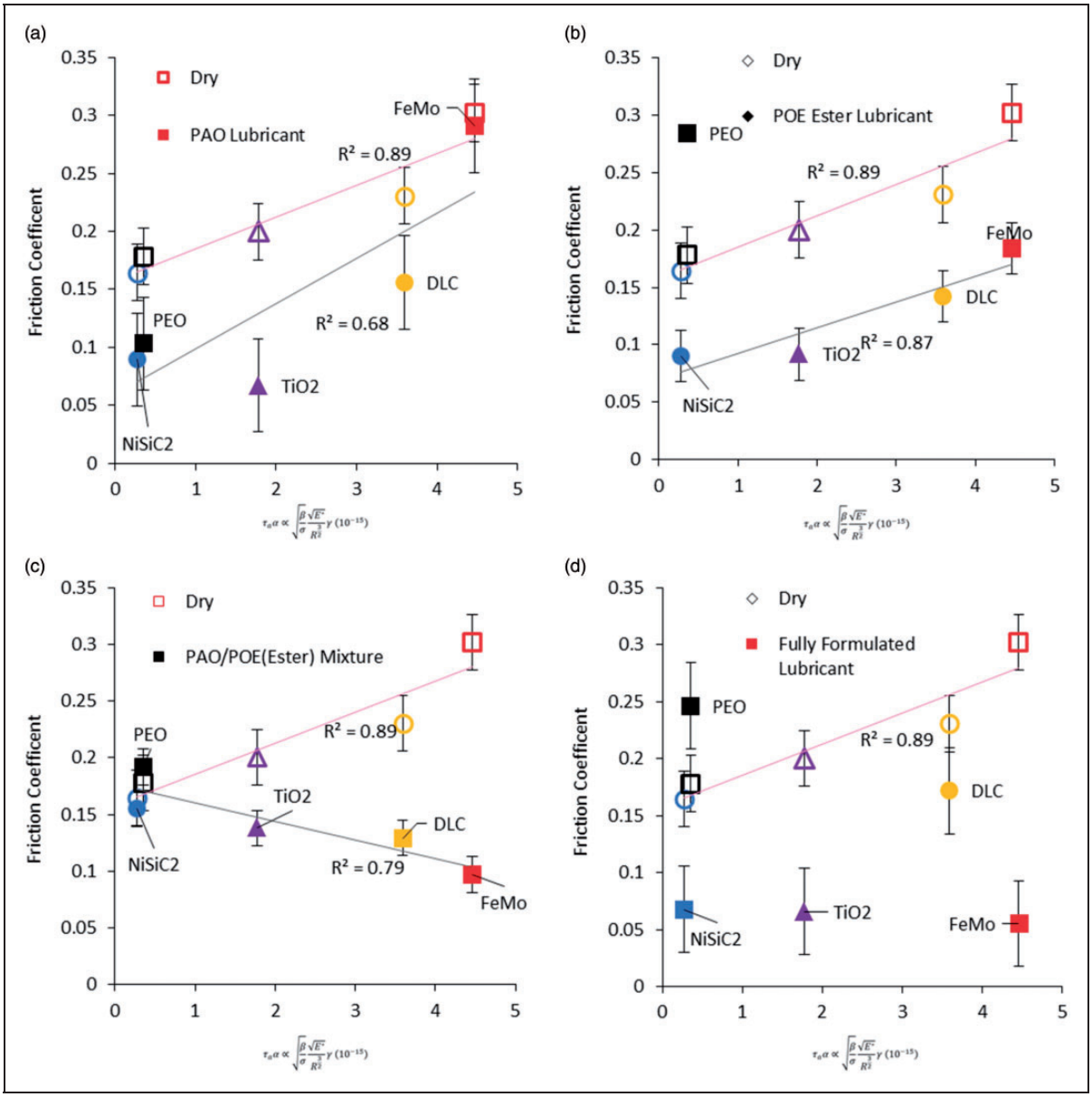

Figure 2. Friction coefficient versus propensity of boundary friction parameter for surfaces lubricated with (a) PAO, (b) POE, (c) PAO/POE mixture and (d) fully formulated oil compared with corresponding dry surface performance.

Table 5. AFM surface roughness measurements.

Sample	Asperity radius of curvature (β) (nm)	RMS roughness (σ) (nm)	Surface energy (γ)
Ni-SiC_2	11.6	1.7	0.002
DLCg	42.0	2.1	0.30
FeMo	6.4	2.9	0.026
TiO_2	22.2	2.6	0.016
PEO	11.4	2.0	0.003

section. For this reason, only the relative performance of the surface types is investigated rather than attempting to quantify individual frictional components. This is appropriate if one assumes that the surface parameters in Table 5 would have the same value relative to one another at the length scale appropriate for the analytical model. In addition, it should be noted that the RMS roughness σ is used to replace the summit height standard deviation σ_s in equation (13) in current study. Such an approximation is deemed reasonable for the limited analysis that follows as it has been shown by Tomanik et al.;[26] that for a range of surfaces, the RMS roughness varies linearly with the peak height standard deviation.

Figure 2(a) shows that the surfaces with a larger value of boundary friction propensity parameter (see equation (13)) demonstrate a minor reduction in the coefficient of friction through the introduction of PAO. This means that PAO, when used in isolation as a lubricant, neither reduces the coefficient of friction by

effectively separating the surfaces (i.e. reducing α) or by lowering the shear strength of the adsorbed film on the surface (i.e. reducing τ_s). For the surfaces, where the boundary friction propensity parameter is low, a significant reduction in the coefficient of friction is observed. This is thought to be primarily due to the displacement of the condensed water layer present on any sample surface by the PAO lubricant. Condensed water films are present on nominally dry surfaces in measurements conducted in a humid environment. The confined water films have been reported to have very high apparent viscosities during confinement.[27] Furthermore, Tambe and Bhushan[14] have shown that the formation of meniscus bridges can influence frictional behaviour of AFM tip-sample conjunction. Therefore, it is proposed that the introduction of the PAO lubricant reduces the shear stress (τ_v), promoting a reduction in friction generated by the sheared fluid in patches of the contact intervened by the presence of a thin fluid film.

In Figure 2(b), the introduction of the POE reduces the coefficient of friction by a similar amount for all the surfaces except for the case of PEO. The reason for a consistent drop in the coefficient of friction for all surface variants is due to a change in the value of (α) as defined by equation (3). This is due to the ester forming a fluid film, promoting an increased gap between the surfaces. The reason for the increased friction of the PEO surface with the introduction of the ester cannot be explained through the current analysis.

Figure 2(c) shows the effect of introducing a mixture of PAO and POE (ester) to the AFM tip-sample conjunction. The results show that the coefficient of friction is significantly reduced for contacts with a high propensity to boundary friction parameter. This indicates that the specified mixed fluid decreases the incidence of boundary friction through either reducing τ_s by the formation of a low shear strength layer on the surface or by reducing (α) through increased contact separation. For low values of the boundary friction propensity parameter, the benefit accrued through contact separating ability of the ester and PAO in isolation (enhanced load carrying capacity) is not maintained by their combined mixture. This highlights the complex behaviour of even simple lubricant-surface systems.

The results for the fully formulated lubricant, shown in Figure 2(d), do not indicate any particular trend with respect to the boundary friction parameter. A similar low coefficient of friction is achieved for each sample surfaces which contains a transition metal (i.e. $NiSiC_2$, FeMo and TiO_2). There is evidence in literature that commonly used inorganic friction modifiers form low friction tribofilms on surfaces containing transition metals.[28–30]

Conclusion

This paper shows the interfacial response depends upon both the fluid in confinement and the properties of the confining surface materials. At the level of asperities, the influence of nanoscale roughness, surface modulus of elasticity and real contact area can be used to determine the dominant frictional behaviour for esters, PAO and a mixture of the two. The ester (POE) is shown to increase the separation of the surfaces (increased load carrying capacity). Consequently, the coefficient of friction is reduced due to a decreased level of boundary interactions. The PAO is shown to reduce the viscous shear in the contact. The fully formulated oil is largely independent of the topographical and material mechanical parameters, with improved frictional performance for all the surfaces containing transition metals (i.e. $NiSiC_2$, FeMo and TiO_2).

The study has shown that lubricant composition can be tailored to meet the requirement of friction reduction for a chosen cylinder bore/liner material for a variety of engine applications. However, it has also been shown that due to the plethora of synergistic or antagonistic interactions between the lubricant species and the surfaces, the simplest of lubricant-surface combinations require detailed combined integrated measurements and contact mechanics analysis.

Acknowledgements

The authors would like to express their gratitude to Capricorn Automotive and the Engineering and Physical Sciences Research Council (EPSRC) under the DTP scheme for the financial support extended to this research.

Declaration of Conflicting Interests

The author(s) declared no potential conflicts of interest with respect to the research, authorship, and/or publication of this article.

Funding

The author(s) received no financial support for the research, authorship, and/or publication of this article.

ORCID iDs

Nicholas Morris https://orcid.org/0000-0001-9463-647X
Ramin Rahmani https://orcid.org/0000-0002-6084-8842

References

1. Akalin O and Newaz GM. Piston ring-cylinder bore friction modeling in mixed lubrication regime: part I: analytical results. *J Tribol* 2001; 123: 211–218.
2. Noorman MT, Assanis DN, Patterson DJ, et al. Overview of techniques for measuring friction using bench tests and fired engines. *SAE Trans* 2000; 890–900.
3. Howell-Smith S, Rahnejat H, King PD, et al. Reducing in-cylinder parasitic losses through surface modification and coating. *Proc IMechE Part D: J Automobile Engineering* 2014; 228: 391–402.
4. Gore M, Morris N, Rahmani R, et al. A combined analytical-experimental investigation of friction in cylinder liner inserts under mixed and boundary regimes of lubrication. *Lubricat Sci* 2017; 29: 293–316.

5. Pidduck AJ and Smith GC. Scanning probe microscopy of automotive anti-wear films. *Wear* 1997; 212: 254–264.
6. Miklozic KT and Spikes HA. Application of atomic force microscopy to the study of lubricant additive films. *J Tribol* 2005; 127: 405–415.
7. Bhushan B, Palacio M and Kinzig B. AFM-based nanotribological and electrical characterization of ultra-thin wear-resistant ionic liquid films. *J Colloid Interf Sci* 2008; 317: 275–287.
8. Campen S, Green JH, Lamb GD, et al. In situ study of model organic friction modifiers using liquid cell AFM: self-assembly of octadecylamine. *Tribol Lett* 2015; 58: 39.
9. Leighton M, Nicholls T, De la Cruz M, et al. Combined lubricant–surface system perspective: multi-scale numerical–experimental investigation. *Proc IMechE, Part J: J Engineering Tribology* 2017; 231: 910–924.
10. Buenviaje C, Ge S and Rafaillovich M. Atomic force microscopy calibration methods for lateral force, elasticity, and viscosity. *Mater Res Soc Symp T – Fund Nanoindent Nanotribol* 1998; 522: 187–192.
11. Styles G, Rahmani R, Rahnejat H, et al. In-cycle and life-time friction transience in piston ring–liner conjunction under mixed regime of lubrication. *Int J Engine Res* 2014; 15: 862–876.
12. Bewsher SR, Leighton M, Mohammadpour M, et al. Boundary friction characterisation of a used cylinder liner subject to fired engine conditions and surface deposition. *Tribol Int* 2019; 131: 424–437.
13. Umer J, Morris N, Leighton M, et al. Nano and micro-scale contact characteristics of tribofilms derived from fully formulated engine oil. *Tribol Int* 2019; 131: 620–630.
14. Tambe NS and Bhushan B. Friction model for the velocity dependence of nanoscale friction. *Nanotechnology* 2005; 16: 2309.
15. Bowden FP and Tabor D. *The friction and lubrication of solids*. Oxford, UK: Clarendon Press, 1950.
16. Gohar R and Rahnejat H. *Fundamentals of tribology*. London, UK: Imperial College Press, 2008.
17. Lantz MA, O'Shea SJ, Welland ME, et al. Atomic-force-microscope study of contact area and friction on NbSe 2. *Phys Rev B* 1997; 55: 10776.
18. Enachescu M, Van den Oetelaar RJA, Carpick RW, et al. Observation of proportionality between friction and contact area at the nanometer scale. *Tribol Lett* 1999; 7: 73.
19. Umer J, Morris N, Leighton M, et al. Asperity level tribological investigation of automotive bore material and coatings. *Tribol Int* 2018; 117: 131–140.
20. Hertz H. Uber den kontakt elastischer korper. *J Reine Angew Math* 1881; 92: 156.
21. Johnson KL. *Contact mechanics*. Cambridge, UK: Cambridge University Press, 1985.
22. Greenwood JA and Williamson JP. Contact of nominally flat surfaces. *Proc R Soc Ser A: Math Phys Sci* 1966; 295: 300–319.
23. Homola AM, Israelachvili JN, McGuiggan PM, et al. Fundamental experimental studies in tribology: the transition from "interfacial" friction of undamaged molecularly smooth surfaces to "normal" friction with wear. *Wear* 1990; 136: 65–83.
24. Fillot N, Berro H and Vergne P. From continuous to molecular scale in modelling elastohydrodynamic lubrication: nanoscale surface slip effects on film thickness and friction. *Tribol Lett* 2011; 43: 257–266.
25. Gosvami NN, Bares JA, Mangolini F, et al. Mechanisms of antiwear tribofilm growth revealed in situ by single-asperity sliding contacts. *Science* 2015; 348: 102–106.
26. Tomanik E, Chacon H and Teixeira G. A simple numerical procedure to calculate the input data of Greenwood-Williamson model of asperity contact for actual engineering surfaces. *Tribol Ser* 2003; 41: 205–215.
27. Ortiz-Young D, Chiu HC, Kim S, et al. The interplay between apparent viscosity and wettability in nanoconfined water. *Nat Commun* 2013; 4: 2482.
28. Vengudusamy B, Green JH, Lamb GD, et al. Behaviour of MoDTC in DLC/DLC and DLC/steel contacts. *Tribol Int* 2012; 54: 68–76.
29. Miyake S, Saito T, Yasuda Y, et al. Improvement of boundary lubrication properties of diamond-like carbon (DLC) films due to metal addition. *Tribol Int* 2004; 37: 751–761.
30. Sun J, Fu ZQ, Zhang W, et al. Friction and wear of Cr-doped DLC films under different lubrication conditions. *Vacuum* 2013; 94: 1–5.

Appendix

Notation

A	Hertzian (apparent) contact area
A_a	asperity contact area
C_F	calibration factor
E^*	effective (equivalent) Young's modulus of elasticity
F_f	friction
h	standardised surface separation
L	applied normal load
R	radius of AFM probe tip
Z_o	equilibrium atomic spacing
α	fraction of real contact area
β	average asperity tip radius of curvature
ε	fractional energy loss
γ	surface energy
η	areal density of asperities
σ	RMS roughness
σ	Summit standard deviation
τ	interfacial shear stress
τ_a	asperity interfacial shear strength
τ_v	viscous shear on confined fluid